Evaluation of Current Tropospheric Mapping Functions by Deep Space Network Very Long Baseline Interferometry

O. J. Sovers and G. E. Lanyi
Tracking Systems and Applications Section

To compare the validity of current algorithms that map zenith tropospheric delay to arbitrary elevation angles, 10 different tropospheric mapping functions are used to analyze the current data base of Deep Space Network Mark III intercontinental very long baseline interferometric (VLBI) data. This analysis serves as a stringent test because of the high proportion of low-elevation observations necessitated by the extremely long baselines. Postfit delay and delay-rate residuals are examined, as well as the scatter of baseline lengths about the time–linear model that characterizes tectonic motion. Among the functions that utilize surface meteorological data as input parameters, the Lanyi 1984 mapping shows the best performance both for residuals and baselines, though the 1985 Davis function is statistically nearly identical. The next best performance is shown by the recent function of Niell, which is based on an examination of global atmospheric characteristics as a function of season and uses no weather data at the time of the measurements. The Niell function shows a slight improvement in residuals relative to Lanyi, but also an increase in baseline scatter that is significant for the California–Spain baseline. Two variants of the Chao mapping function, as well as the Chao tables used with the interpolation algorithm employed in the Orbit Determination Program software, show substandard behavior for both VLBI residuals and baseline scatter. The length of the California–Australia baseline (10,600 km) in the VLBI solution can vary by as much as 5 to 10 cm for the 10 mapping functions.

I. Introduction

The tropospheric delay is one of the most poorly understood components in the theoretical model of very long baseline interferometric (VLBI) observables. This was first realized at least a decade ago, and numerous attempts have been made during the past 10 years to improve tropospheric modeling. These include the two high-quality mapping functions of Lanyi [1] and Davis et al. [2], the model of tropospheric turbulence by Treuhaft and Lanyi [3], and a plethora of mapping functions developed since the mid-1980s. Recent reviews by Gallini [4] and Estefan and Sovers [17] provide a good summary.

During the past decade at JPL, the Lanyi tropospheric mapping function has been part of the VLBI theoretical model in the MODEST software [5], the GPS models in the GIPSY software [6], and the 1992 International Earth Rotation Service (IERS) Standards [7]. The Orbit Determination Program (ODP)

1

still uses the much older Chao tables.[1] Other VLBI groups have employed, in succession, the Davis (CfA) [2], Herring (MTT) [8], and Niell (NMF)[2] [9] mapping functions. In view of the multitude of recent new mapping functions, it is of interest to determine whether the decade-old JPL VLBI tropospheric model is still state of the art, as it was when first introduced in 1984. To this end, some simple tests were devised to evaluate the performance of the newer mapping functions, as well as the older Chao algorithms, for a typical data set of DSN VLBI observations. The results also have bearing on the adequacy of the current ODP tropospheric model.

The next section describes the VLBI analyses that were carried out to evaluate the performance of 10 variants of tropospheric mapping algorithms. The data base consists of all currently processed DSN Mark III VLBI observations since their inception in late 1988. The quantities examined are the postfit residuals, as a function of elevation angle, and the scatter of daily baseline lengths about the linear model of tectonic plate motion. Conclusions and recommendations for theoretical modeling in VLBI and orbit analyses are presented in the last section.

II. Mapping Function Comparisons

Tests, using VLBI measurements with DSN antennas, were devised to evaluate the performance of a variety of tropospheric mapping functions carried out during the past decade. These were typically 24-hr observing sessions using two antennas separated by either of the two intercontinental baselines (approximately 8,400 or 10,600 km), looking over as large a region of the sky as permitted by mutual-source visibility. Because the extreme baseline length is a large fraction of an Earth diameter, the region of the sky accessible at either site was severely limited, and numerous observations were made at the lower elevation limits of the antennas (approximately 6 deg). These low-elevation observations help to decorrelate zenith delays at the two stations in data analyses, but require good accuracy in the tropospheric mapping at low-elevation angles. While tropospheric delay is also an important part of the theoretical model in orbit determination with the ODP software [17],[3] similar tests for the Doppler and range observables in spacecraft tracking are precluded by the lack of accepted observations below 15-deg elevations, which is the region most sensitive to details of the mapping algorithm.

To avoid the possibility of drawing false conclusions induced by the much higher system noise level of the early observations (approximately 10 cm for Mark I, 2 cm for Mark III), only a subset of the VLBI data was selected for detailed analysis. It included all the newer data, recorded with Mark III data acquisition systems. The data spanned the time period 1988 to 1993; a total of 11,897 delay and delay-rate pairs was used. A standard VLBI parameter estimation fit was performed. The estimated parameters included positional coordinates of 283 radio sources, a pair of nutation angle offsets for each session (longitude and obliquity), and station coordinates for each overseas station (Australia and Spain) for each of the 61 sessions. The right ascension of one source, the nutation model on one day, and the Goldstone station coordinates were kept fixed. A new value of the zenith tropospheric value was estimated every 2 hr at each station. Correlations among the delay and delay-rate observables due to tropospheric fluctuations were ignored here, but will be considered in a future article. More details of both the DSN data-acquisition and parameter-estimation procedures have been previously published [10,11]. MacMillan and Ma [12] recently performed a similar evaluation for the Chao, Davis, Herring, and Ifadis tropospheric models, using the NASA Crustal Dynamics Project (CDP) and National Oceanic and Atmospheric Administration (NOAA) International Radio Interferometric Surveying (IRIS) data bases.

---

[1] C. C. Chao, "Improved Tropospheric Mapping Tables (Including Bending Effect) for SATODP," JPL Interoffice Memorandum 391.3-637 (internal document), Jet Propulsion Laboratory, Pasadena, California, December 28, 1972.

[2] A. E. Niell, *Global Mapping Functions for the Atmospheric Delay at Radio Wavelengths*, Haystack Observatory, Westford, Massachusetts, a draft report received as a personal communication, March 31, 1994.

[3] N. A. Mottinger, "Reflections on Refraction—A Historical Overview of the Tropospheric Refraction Model in the ODP," JPL Interoffice Memorandum 314.10-385 (internal document), Jet Propulsion Laboratory, Pasadena, California, January 18, 1984.

A postfit analysis estimates time–linear variation of the station coordinates, as well as the Goldstone–overseas baseline lengths. Such fits and postfit baseline analyses were repeated for each of 10 tropospheric mapping functions, with all other aspects of modeling and parameter estimation (the latter with one exception) being identical. The mapping functions are listed in Table 1. For those functions requiring surface meteorological measurements (nos. 4 through 9), such data were taken from the Deep Space Communications Complex (DSCC) Media Calibration Subsystem data base.[4] Temperature lapse rates had seasonal variations at the Australia and Spain stations,[5] while the default −6.5 K/km was used for Goldstone. The two remaining atmospheric parameters (inversion and tropopause heights) were assigned default values of 1.25 and 12.2 km, respectively. The "Lanyi estimated" function requires some additional explanation. It uses the Lanyi 1984 function to accurately map the zenith delays, based on the available tabulated surface and balloon meteorological data. A crude single-parameter approximation is then used to account for the effect of deviations between the real and tabulated meteorological data on the mapping function [5]. One such parameter is estimated at each station for every observing session.

Table 1. Troposphere mapping functions used in fits to DSN VLBI data.

Mapping function	JPL VLBI archive ID	Reference	Comments
1 = Chao original	152	[13]	
2 = Chao revised	153	[14]	Revised constants
3 = Chao tables	154	Footnote 1	Tables used in ODP
4 = Lanyi standard	151	[1]	
5 = Lanyi updated	155	—a	Geometry and gravity curvature corrections
6 = Lanyi estimated	156	[5]	One parameter/station estimated per 24-hr experiment
7 = Davis	158	[2]	Alias CfA
8 = Ifadis	157	[15]	
9 = Herring	159	[8]	Alias MTT
10 = Niell	160	[9]	Alias NMF

a G. E. Lanyi, "Tropospheric Propagation Delay Effects for Radio Waves," JPL Interoffice Memorandum 335.1-156 (internal document), Jet Propulsion Laboratory, Pasadena, California, November 15, 1983.

Our examination of tropospheric mapping functions includes

(1) Comparison of the total tropospheric delays given by the various mapping functions for the DSN sites for the particular subset of meteorological conditions prevailing at the times of the VLBI measurements.

(2) Comparison of VLBI delay and delay-rate residuals and baseline-length scatter resulting from multiparameter estimation in model fits to the VLBI observables.

The first category thus reflects the effect on the mapping functions of the elevation distributions and weather conditions at the times of the VLBI experiments, while the second category is a quantitative

---

[4] T. F. Runge, *Troposphere Calibration Software*, JPL SRD-NVI-5454-OP (internal document), Jet Propulsion Laboratory, Pasadena, California, August 31, 1993.

[5] M. A. Smith, "Analysis of Meteorological Balloon Data," JPL Interoffice Memorandum 335.6-92-023 (internal document), Jet Propulsion Laboratory, Pasadena, California, July 27, 1992.

assessment of how well each mapping function represents the data. These two categories of tests are described in turn in the two following subsections.

A. Statistics of Mapping Function Delay Values

Direct comparisons of mapping functions under varying atmospheric conditions yield voluminous data, most of which will not be presented here. They are in partial agreement with the results presented by Mendes and Langley [16].[6] Discrepancies between tropospheric delays calculated with different mapping functions generally increase rapidly with decreasing elevation angles below 20 deg. In the extreme case, the difference reaches approximately 10 cm of tropospheric delay at the DSN lower observational limit of 6 deg. A histogram of the elevation angles of the DSN VLBI observations is shown in Fig. 1. The distribution is seen to peak between 10 and 15 deg, with more than half of the observations being below a 30-deg elevation at one or both ends of the baseline. This distribution of observations with elevation angle and the magnitude of the differences between the mapping functions are generally consistent with the postfit analyses.
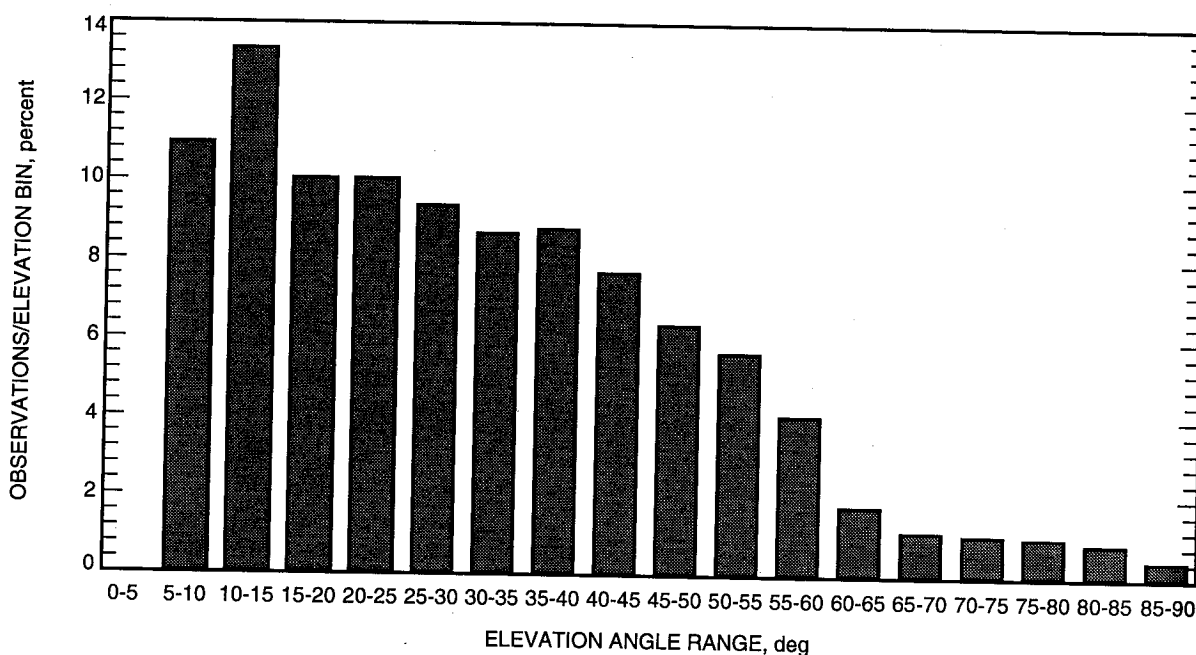

Fig. 1. Histogram of elevation angle distributions of DSN Mark III VLBI observations.

Figure 2 shows the total delay differences as a function of elevation angle for the Davis and Niell mapping functions. The Davis function is shown because it gives the closest fit results to Lanyi; the Niell function was not available for the initial work of Mendes and Langley and appears to show a performance nearly equivalent to that of the Lanyi mapping function. All tropospheric delay values were evaluated at each station for all 11,897 observations, using observed values for any required surface meteorological data. The results were placed in 0.5-deg bins for elevations lower than 20 deg and 1-deg bins above 20 deg; the error bars in Fig. 2 correspond to the standard deviation from the average in each bin. The differences are seen to be as large as 3 cm for Niell minus Lanyi just above a 6-deg elevation and to decrease rapidly toward zero when approaching 20 deg. The scatter within each bin approaches 1 cm below 10 deg for both functions. Note that the Davis–Lanyi differences have a negative region of 1–2 mm at mid-elevations. It should be noted that the plots in Fig. 2 represent statistical rather than exact mapping function comparisons. The Niell mapping function internally contains statistical

---

[6] Better agreement was not attained because in some of the Mendes and Langley comparisons not all of the needed meteorological data were used.

4

averages of atmospheric parameters; for the Davis and Lanyi mapping functions, DSN statistical averages of atmospheric parameters were used, e.g., monthly averages of zenith delays. Since daily values of the surface pressure were used for the Davis function, there could be a small discrepancy (a few millimeters at 6 deg) in Fig. 2(a) due to the dependence of the bending effect on the zenith delay or, equivalently, on the surface pressure.
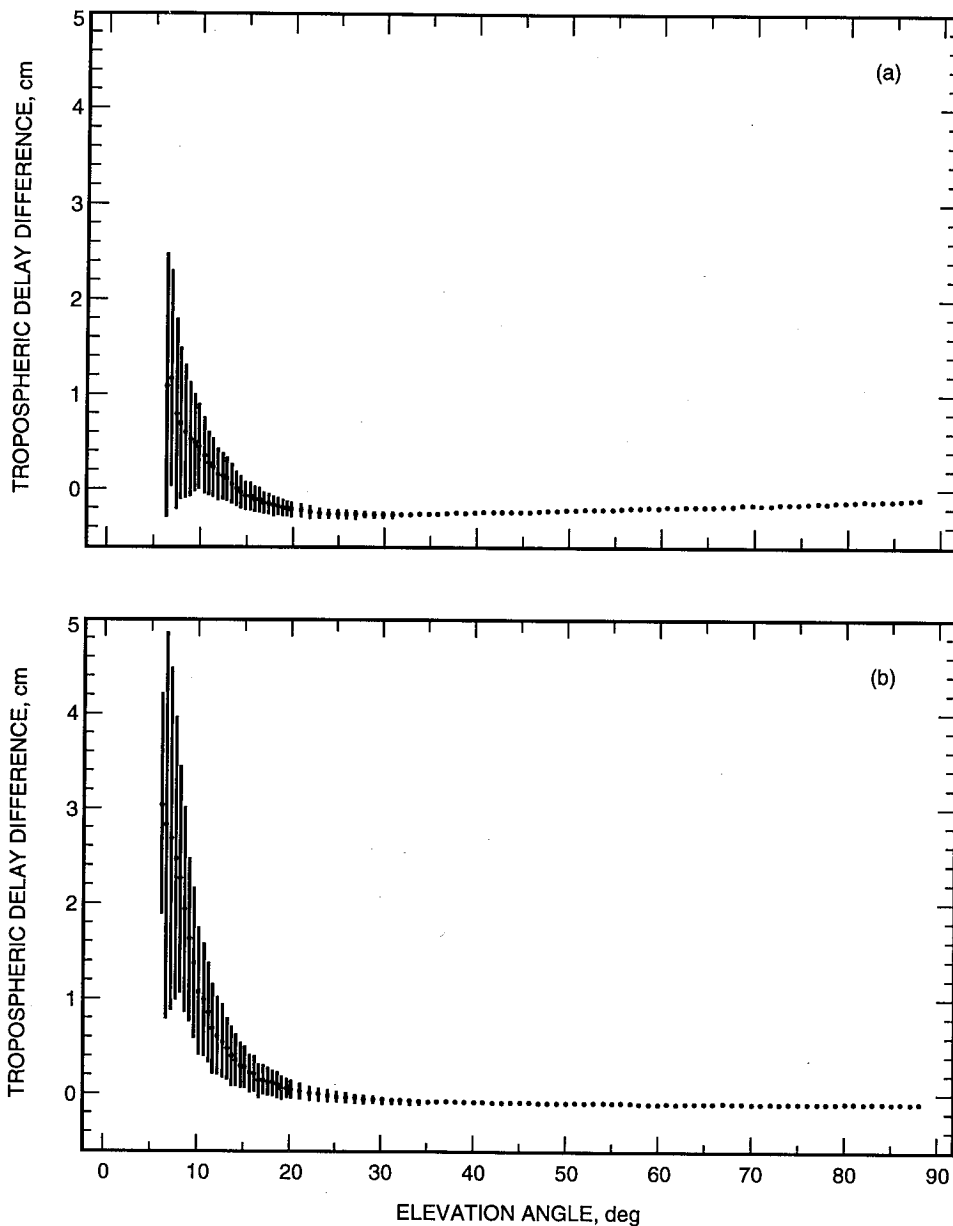

Fig. 2. Tropospheric delay difference versus elevation angle for DSN Mark III VLBI observations: (a) Davis minus Lanyi and (b) Niell minus Lanyi mapping functions. Each error bar is the standard deviation from the mean of all values in each elevation bin.

B. Statistics of Postfit Residuals

The postfit quantities that were examined included the delay and delay-rate residuals, the "baseline scatter" and χ^2 for a time–linear fit to baselines estimated independently for each observing session, and

the baseline length bias (change in baseline length at a given epoch induced by a change in the mapping function). Our criteria for a good mapping function are small values for the residuals and the baseline scatter. Differences in the average angular dependence of the mapping functions, as well as in the resulting baseline scales, can point to particular elevation ranges or baselines that are not properly modeled.

Table 2 shows the rms delay and delay-rate residuals and total χ^2's for the 10 VLBI fits. Normalized χ^2 values are not shown because of the uncertainty in partitioning parameters between the two observable types. The "improvement" columns in this table (as well as in Tables 3 and 4) contain the signed rms difference between the residuals given by each mapping function and Lanyi standard. Focusing first on the residual results in Table 2, we see that the mapping functions fall into three broad groups. Both Chao functions and the Chao tables produce fits to VLBI data that are definitely inferior, especially for delay rates. All other functions do not differ by more than a few picoseconds in delay residuals from the Lanyi function and its variants. Only the Niell and Ifadis functions, and Lanyi with parameters estimated, improve both the delay and delay-rate residuals. As may be seen from the subsequent results as well, the Niell and Ifadis functions show very similar behavior.

Table 2. Mark III VLBI residuals.

Mapping function[a]	Delay (D)		Delay rate (DR)		Improvement[b]	
	rms, psec	χ^2	rms, fsec/sec	χ^2	D, psec	DR, fsec/sec
1	71.6655	9665	131.512	13,140	-19.4	-38.2
2	69.2404	8932	126.494	11,883	-5.9	-12.7
3	70.4522	9176	154.737	21,456	-14.3	-90.0
4	68.9867	8835	125.856	11,701	—	—
5	69.0001	8838	125.869	11,702	-1.4	-1.8
6	68.8222	8784	125.314	11,599	$+4.8$	$+12.7$
7	69.0492	8844	126.315	11,788	-2.9	-10.8
8	68.9374	8837	125.762	11,717	$+2.6$	$+4.9$
9	69.0331	8838	125.767	11,695	-2.5	$+4.7$
10	68.9273	8813	125.608	11,682	$+2.9$	$+9.4$

[a] Mapping function definitions are provided in Table 1.
[b] Relative improvement is based on mapping function 4.

To assess the behavior of each tropospheric mapping function in various elevation angle ranges, the delay residuals were divided into the six elevation bins shown in Table 3: observations below 10 deg, 5-deg bins up to 30 deg, and observations from 30 deg to zenith. Table 3 gives the raw results and relates them to the Lanyi standard function. It is seen that the Niell and Ifadis (and Lanyi with estimated parameters) improvements in residuals are not uniform across the range of elevations. They do well at very low angles, but not in the 10- to 15-deg and 25- to 30-deg ranges (this holds for most of the newer functions). No extraordinary elevation-partitioned results are seen, with one exception: It can be noted that the Lanyi parameters-estimated function apparently achieves reductions in residuals by improving the mapping function shape at very low elevations.

Table 4 shows baseline length results from the VLBI data analyses. It is seen that any departure from the standard Lanyi mapping function increases the baseline scatter and χ^2 per degree of freedom (χ^2_ν) (with the exception of Davis on the California–Spain [DSS 15–DSS 65] baseline), sometimes by substantial amounts. The statistical significance of these differences can be inferred from the formal uncertainties of χ^2_ν. The number of degrees of freedom N in the California–Australia (DSS 15–DSS 45) and California–Spain fits are 30 and 27, respectively. Thus, the standard deviation of the normalized χ^2,

$\sigma_{\chi_\nu^2}$, is approximately $(2/N)^{1/2} = 0.26$ and 0.27. Even for the best fits, however, χ_ν^2 shows substantial departures from unity. This originates both from model inadequacies and underestimated observable errors. We assume that the best fits correspond to the best modeling, and that in this case modeling errors and error underestimates contribute equally to the increased χ^2. According to this assumption, the χ^2 value corresponding to the underestimated errors is $1 + (\chi^2 - 1)/2$. Consequently, to obtain a more realistic error for χ_ν^2, we multiply the formal $\sigma_{\chi_\nu^2}$ by this estimated quantity, 1.3 and 1.6 for the two baselines, respectively. This gives $\sigma_{\chi_\nu^2} = 0.34$ and 0.44, which are the error bars used in Figs. 3(a) and (b). Since all fits are based on identical data, the statistical significance of the difference between different solutions is measured by the standard deviation of χ_ν^2 itself, i.e., 0.34 or 0.44.

Table 3. Delay residuals by elevation range.

Mapping function[a]	Range of elevation angles, deg					
	0–10	10–15	15–20	20–25	25–30	30–90
	Delay residuals, psec					
1	98.993	76.114	66.665	64.213	65.090	66.386
2	94.562	73.217	65.754	62.232	62.562	64.346
3	97.358	74.320	66.923	62.694	62.537	65.477
4	94.117	72.692	65.883	62.025	61.914	64.221
5	94.134	72.708	65.904	62.036	61.911	64.235
6	93.679	72.807	65.770	61.903	61.938	64.000
7	94.419	72.716	65.873	61.990	61.900	64.267
8	94.049	72.782	65.632	61.965	62.171	64.121
9	94.174	72.918	65.777	62.027	62.173	64.210
10	93.994	72.772	65.741	61.938	62.151	64.104
	Improvement over Lanyi standard in quadrature, psec[b]					
1	−30.7	−22.6	−10.2	−16.6	−20.1	−16.8
2	−9.2	−8.8	+4.1	−5.1	−9.0	−4.0
3	−24.9	−15.5	−11.8	−9.1	−8.8	−12.8
4	—	—	—	—	—	—
5	−1.8	−1.5	−1.7	−1.2	+0.6	−1.3
6	+9.1	−4.1	+3.9	+3.9	−1.7	+5.3
7	−7.5	−1.9	+1.1	+2.1	+1.3	−2.4
8	+3.6	−3.6	+5.7	+2.7	−5.6	+3.6
9	−3.3	−5.7	+3.7	−0.5	−5.7	+1.2
10	+4.8	−3.4	+4.3	+3.3	−5.4	+3.9

[a] Mapping function definitions are provided in Table 1.
[b] Relative improvement is based on mapping function 4.

The differences are due to mapping errors and are seen to be highly significant for the group of three Chao functions versus Lanyi. They are marginally significant for the remaining functions on the California–Australia baseline, and $> 2\sigma_{\chi_\nu^2}$ significant for Ifadis, Herring, and Niell versus Lanyi on the California–Spain baseline. The Ifadis, Herring, and Niell mapping functions all worsen the scatter by at least 10 mm on both baselines. The Davis function resembles Lanyi most closely in regard to scatter.

Table 4. Baseline-length results.

Mapping function[a]	Baseline							
	DSS 15–DSS 45[b]		DSS 15–DSS 65		DSS 15–DSS 45[c,d]		DSS 15–DSS 65	
	δ_B	χ^2_ν	δ_B	χ^2_ν	$\Delta\delta_B$[e]	β_B	$\Delta\delta_B$	β_B
1	49.4	5.8	24.6	8.0	−40.8	173	−20.6	172
2	42.1	4.2	24.3	7.8	−31.5	90	−20.3	112
3	38.0	3.1	24.8	7.9	−25.8	26	−20.9	9
4	27.9	1.7	13.4	2.2	—	—	—	—
5	27.9	1.7	13.4	2.2	0.0	−3	0.0	−2
6	38.4	1.7	19.9	3.0	−26.4	6	−14.7	6
7	28.1	1.6	13.9	2.3	−3.3	20	−3.7	15
8	29.9	2.0	17.3	3.8	−10.8	62	−10.9	41
9	32.5	2.3	17.1	3.7	−16.7	61	−10.6	40
10	30.3	2.0	16.2	3.3	−11.8	58	−9.1	45

[a] Mapping function definitions are provided in Table 1.
[b] δ_B = scatter (mm).
[c] $\Delta\delta_B$ = improvement of scatter (mm).
[d] β_B = bias (mm).
[e] Relative improvement is based on mapping function 4.

The Lanyi map with parameters estimated achieves its residual improvement at the expense of increases in baseline scatter of 26 and 15 mm. The purpose of this fit is to model any remaining variation in the mapping function due to inaccurate atmospheric modeling; indeed, the rms observable residuals decrease. This improvement appears to be achieved by propagating the delay residual errors into systematic baseline errors. The mechanism is poorly understood and is currently under further study. Most mapping functions also yield substantial baseline length biases relative to Lanyi 1984, ranging from 20 to 62 mm for the California–Australia 10,600-km baseline (the Chao tables do very well in this regard, shifting the scale by only 26 mm).

III. Conclusions

Based on the comparisons discussed in the previous section, a number of conclusions can be drawn. In the absence of more generalized testing, these conclusions should be regarded as limited to mapping the tropospheric delays at the three DSN sites. The statistical significance of differences among the mapping functions is tied to the residual scatter of these particular DSN VLBI fits. First, all three variants of the Chao mappings are very inadequate. They produce postfit residual and baseline scatter values that are inferior by many centimeters relative to the more modern functions. Second, the 1984 Lanyi mapping function is still, by a small margin, equivalent or superior to all the newer algorithms developed during the intervening decade. Third, those mapping functions that employ no or limited surface meteorological data are either equivalent to or slightly worse than the Lanyi function. Some of their deficiencies may be due to the fact that their functional forms are based on atmospheric profiles measured at predominantly North American sites. Finally, of the functions using minimal or no surface data, either the Ifadis or Niell function produces tropospheric models of DSN VLBI measurements that are nearly equal in quality to those given by the Lanyi mapping function on the California–Australia baseline, but worse on the California–Spain baseline.

Of the three major JPL astrometric/geodetic/navigational software packages, MODEST and the GPS analysis software GIPSY have always used the Lanyi 1984 function for tropospheric delay calibration. The former also has options to employ any of the models discussed in the present article. The Chao table formulation in ODP is seen to be grossly inadequate, especially at low elevation angles, and should be updated to one of the modern functions.
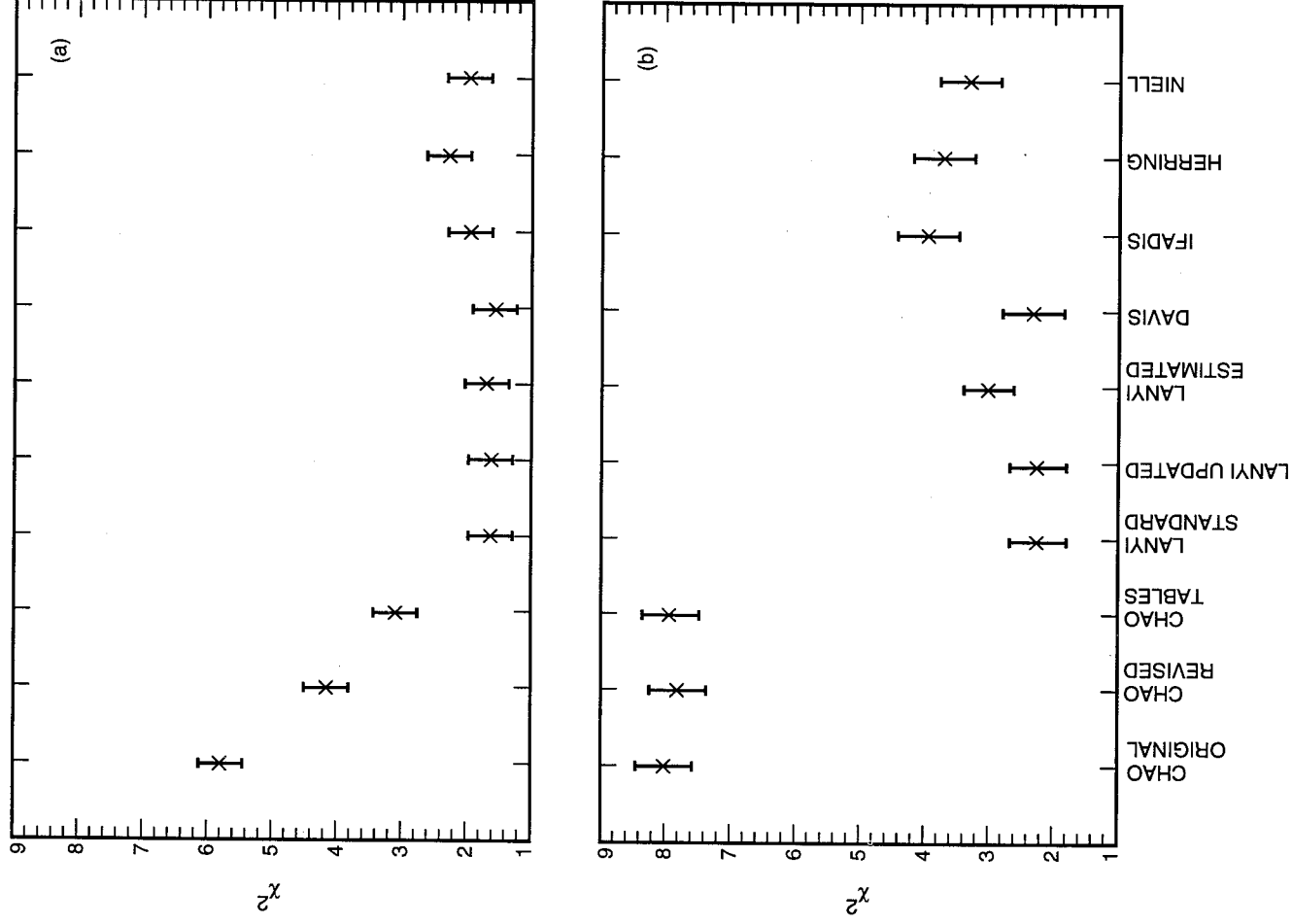

Fig. 3. Normalized χ^2 of residuals from a linear fit to baseline lengths versus time for (a) the California–Australia baseline and (b) the California–Spain baseline. See text for explanation of error bars.

Acknowledgments

References

[1] G. E. Lanyi, "Tropospheric Delay Effects in Radio Interferometry," *The Telecommunications and Data Acquisition Progress Report 42-78, vol. April–June 1984*, Jet Propulsion Laboratory, Pasadena, California, pp. 152–159, August 15, 1984.

[2] J. L. Davis, T. A. Herring, I. I. Shapiro, A. E. E. Rogers, and G. Elgered, "Geodesy by Radio Interferometry: Effects of Atmospheric Modeling Errors on Estimated Baseline Length," *Radio Science*, vol. 20, pp. 1593–1607, 1985.

[3] R. N. Treuhaft and G. E. Lanyi, "The Effect of the Dynamic Wet Troposphere on Radio Interferometric Measurements," *Radio Science*, vol. 22, pp. 251–265, March–April 1987.

[4] T. E. Gallini, *A Survey of Tropospheric Refraction Models*, Aerospace Report TOR-94(4488)-11, The Aerospace Corporation, El Segundo, California, April 20, 1994.

[5] O. J. Sovers and C. S. Jacobs, *Observation Model and Parameter Partials for the JPL VLBI Parameter Estimation Software "MODEST"-1994*, JPL Publication 83-39, Rev. 5, Jet Propulsion Laboratory, Pasadena, California, August 1994.

[6] O. J. Sovers and J. S. Border, *Observation Model and Parameter Partials for the JPL Geodetic GPS Modeling Software "GPSOMC,"* JPL Publication 87-21, Rev. 2, Jet Propulsion Laboratory, Pasadena, California, June 15, 1990.

[7] *IERS Standards, IERS Technical Note 13*, edited by D. D. McCarthy, International Earth Rotation Service, Paris, France, 1992.

[8] T. A. Herring, "Modeling Atmospheric Delays in the Analysis of Space Geodetic Data," *Refraction of Transatmospheric Signals in Geodesy*, edited by J. C. De-Munck and T. A. Th. Spoelstra, The Netherlands Commission on Geodesy, Delft, Netherlands, 1992.

[9] A. E. Niell, "A New Approach for the Hydrostatic Mapping Function," *Proceedings of the International Workshop for Reference Frame Establishment and Technology Development in Space Geodesy*, Communications Research Laboratory, Koganei, Tokyo, Japan, pp. 61–68, January 1993.

[10] O. J. Sovers, C. D. Edwards, C. S. Jacobs, G. E. Lanyi, K. M. Liewer, and R. N. Treuhaft, "Astrometric Results of 1978-1985 Deep Space Network Radio Interferometry: The JPL 1987-1 Extragalactic Source Catalog," *Astron. J.*, vol. 95, pp. 1647–1658, 1988.

[11] O. J. Sovers, "JPL 1990-3: A 5-nrad Extragalactic Source Catalog Based on Combined Radio Interferometric Observations," *The Telecommunications and Data Acquisition Progress Report 42-106, vol. April–June 1991*, Jet Propulsion Laboratory, Pasadena, California, pp. 364–383, August 15, 1991.

[12] D. S. MacMillan and C. Ma, "Evaluation of Very Long Baseline Interferometry Atmospheric Modeling Improvements," *J. Geophys. Res.*, vol. 99, no. B1, pp. 637–651, 1994.

[13] C. C. Chao, *The Troposphere Calibration Model for Mariner Mars 1971*, Technical Report 32-1587, Jet Propulsion Laboratory, Pasadena, California, pp. 61–76, March 1974.

[14] C. C. Chao, "New Tropospheric Range Corrections With Seasonal Adjustment," *The DSN Progress Report for September and October 1971*, Technical Report 32-1526, vol. VI, Jet Propulsion Laboratory, Pasadena, California, pp. 67–82, December 15, 1971.

[15] I. I. Ifadis, *The Atmospheric Delay of Radio Waves: Modeling the Elevation Dependence on a Global Scale*, Technical Report 38L, Chalmers University of Technology, Göteborg, Sweden, 1986.

[16] V. B. Mendes and R. B. Langley, "Modeling the Tropospheric Delay From Meteorological Surface Measurements: Comparison of Models" (abstract), *EOS Transactions*, vol. 75, no. 16, p. 105, May 23–27, 1994.

[17] J. A. Estefan and O. J. Sovers, *A Comparative Survey of Current and Proposed Tropospheric Refraction-Delay Models for DSN Radio Metric Data Calibration*, JPL Publication 94-24, Jet Propulsion Laboratory, Pasadena, California, October 1994.